



HAL
open science

Towards fully electrically controlled domain-wall logic

B B Vermeulen, E. Raymenants, V T Pham, S. Pizzini, B. Sorée, K. Wostyn,
S. Couet, V D Nguyen, K. Temst

► **To cite this version:**

B B Vermeulen, E. Raymenants, V T Pham, S. Pizzini, B. Sorée, et al.. Towards fully electrically controlled domain-wall logic. *AIP Advances*, 2024, 14 (2), pp.025030. 10.1063/9.0000811. hal-04485431

HAL Id: hal-04485431

<https://hal.science/hal-04485431>

Submitted on 1 Mar 2024










HAL is a multi-disciplinary open access archive for the deposit and dissemination of scientific research documents, whether they are published or not. The documents may come from teaching and research institutions in France or abroad, or from public or private research centers.

L'archive ouverte pluridisciplinaire **HAL**, est destinée au dépôt et à la diffusion de documents scientifiques de niveau recherche, publiés ou non, émanant des établissements d'enseignement et de recherche français ou étrangers, des laboratoires publics ou privés.

RESEARCH ARTICLE | FEBRUARY 16 2024

Towards fully electrically controlled domain-wall logic

Special Collection: [68th Annual Conference on Magnetism and Magnetic Materials](#)

B. B. Vermeulen ; E. Raymenants ; V. T. Pham ; S. Pizzini ; B. Sorée ; K. Wostyn ;
S. Couet ; V. D. Nguyen ; K. Temst 




AIP Advances 14, 025030 (2024)


<https://doi.org/10.1063/9.0000811>



CrossMark



Biomicrofluidics
Special Topic:
Microfluidic Biosensors
Submit Today



Towards fully electrically controlled domain-wall logic

Cite as: AIP Advances 14, 025030 (2024); doi: 10.1063/9.0000811

Submitted: 4 October 2023 • Accepted: 20 January 2024 •

Published Online: 16 February 2024



View Online



Export Citation



CrossMark

B. B. Vermeulen,^{1,2,a}  E. Raymenants,¹  V. T. Pham,^{1,3}  S. Pizzini,³  B. Sorée,^{1,4,5}  K. Wostyn,¹ 
S. Couet,¹  V. D. Nguyen,^{1,b}  and K. Temst^{1,2} 

AFFILIATIONS

¹ Interuniversity Microelectronics Center (IMEC), 3001 Leuven, Belgium

² KU Leuven, QSP Division, Celestijnenlaan 200 D - Box 2414, 3001 Leuven, Belgium

³ Univ. Grenoble Alpes, CNRS, Institut Néel, 38042 Grenoble, France

⁴ KU Leuven, ESAT-INSYS Division, Kasteelpark Arenberg 10, 3001 Leuven, Belgium

⁵ Universiteit Antwerpen, Departement of Physics, Groenenborgerlaan 171, 2020 Antwerp, Belgium

Note: This paper was presented at the 68th Annual Conference on Magnetism and Magnetic Materials.

^{a)} Author to whom correspondence should be addressed: bob.vermeulen@imec.be

^{b)} Electronic mail: van.dai.nguyen@imec.be

ABSTRACT

Utilizing magnetic tunnel junctions (MTJs) for write/read and fast spin-orbit-torque (SOT)-driven domain-wall (DW) motion for propagation, enables non-volatile logic and majority operations, representing a breakthrough in the implementation of nanoscale DW logic devices. Recently, current-driven DW logic gates have been demonstrated via magnetic imaging, where the Dzyaloshinskii-Moriya interaction (DMI) induces chiral coupling between perpendicular magnetic anisotropy (PMA) regions via an in-plane (IP) oriented region. However, full electrical operation of nanoscale DW logic requires electrical write/read operations and a method to pattern PMA and IP regions compatible with the fabrication of PMA MTJs. Here, we study the use of a Hybrid Free Layer (HFL) concept to combine an MTJ stack with DW motion materials, and He⁺ ion irradiation to convert the stack from PMA to IP. First, we investigate the free layer thickness dependence of 100-nm diameter HFL-MTJ devices and find an optimal CoFeB thickness, from 7 to 10 Å, providing high tunneling magnetoresistance (TMR) readout and efficient spin-transfer torque (STT) writing. We then show that high DMI materials, like Pt/Co, can be integrated into an MTJ stack via interlayer exchange coupling with the CoFeB free layer. In this design, DMI values suitable for SOT-driven DW motion are measured by asymmetric bubble expansion. Finally, we demonstrate that He⁺ irradiation reliably converts the coupled free layers from PMA to IP. These findings offer a path toward the integration of fully electrically controlled DW logic circuits.

© 2024 Author(s). All article content, except where otherwise noted, is licensed under a Creative Commons Attribution (CC BY) license (<http://creativecommons.org/licenses/by/4.0/>). <https://doi.org/10.1063/9.0000811>

I. INTRODUCTION

Domain-wall (DW) logic, where information is encoded in magnetic domains, is currently explored as a promising candidate for low power and compact logic circuits via the implementation of majority gates.^{1,2} DW logic can benefit from the state-of-the-art magnetic tunnel junction (MTJ) technology for electrical writing and reading of DWs.^{3,4} Moreover, fast spin-orbit-torque (SOT)-driven DW motion enables energy-efficient information processing from input to output.⁵⁻⁷

In 2020, Luo *et al.* demonstrated SOT-driven DW inverter (i.e., NOT gate) and DW NAND/NOR logic gates in a Pt/Co/AlO_x stack with perpendicular magnetic anisotropy (PMA).⁸ The DW inverter operation is enabled by a region with in-plane (IP) magnetization inside the out-of-plane (OOP) magnetic tracks. The interfacial Dzyaloshinskii-Moriya interaction (DMI)^{9,10} from the Pt/Co interface induces chiral coupling that leads to an anti-parallel alignment of OOP regions separated by a narrow IP region.¹¹ When a DW is driven through an IP region, it is inverted from down/up to up/down or inversely.

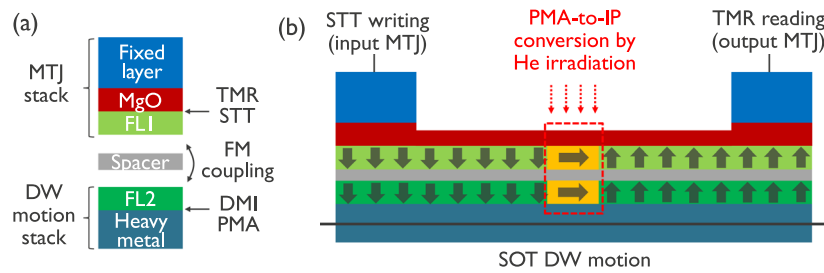


FIG. 1. (a) Hybrid Free Layer concept consisting of FL1 based on CoFeB/MgO for high TMR read and efficient STT write, and FL2 based on Pt/Co with high DMI and PMA for fast SOT DW motion. (b) Schematic of a DW logic device based on the HFL concept and a He⁺ irradiation treatment to pattern in-plane magnetic regions.

In this article, we demonstrate solutions to improve this DW logic concept in order to enable nanoscale electrical writing and reading of DWs with MTJs, which is required for a real application potential.

We first study MTJ write/read capabilities in 100-nm pillars using the Hybrid Free Layer (HFL) concept,³ which combines SOT DW motion materials with an MTJ stack. This concept was initially studied to increase the thermal stability of STT-MRAM memory cells,¹² and is applied here to DW devices to enable electrical control. The HFL consists of two free layers (FLs) ferromagnetically (FM) coupled via interlayer exchange coupling through a spacer [see Fig. 1(a)]. FL1, typically CoFeB/MgO,¹³ provides efficient spin-transfer torque (STT) for writing and high tunneling magnetoresistance (TMR) for reading. FL2, typically Pt/Co, offers PMA and DMI for chiral DWs, enabling fast SOT-driven DW motion. Additionally, we demonstrate that blanket HFL stacks also possess adequate DMI.

We then study He⁺ ion irradiation as a method to convert the HFL from PMA to IP in order to enable the fabrication of DW logic gates [see Fig. 1(b)]. Indeed, since the DW track is part of the PMA MTJ stack, it is required to have PMA. Instead of converting from IP to OOP with the local oxidation of Pt/Co/Al,¹¹ He⁺ irradiation enables the conversion from OOP to IP by inducing gentle intermixing of the interfaces, leading to a reduction of the interfacial PMA.^{14–17} We demonstrate this method by global irradiation of blanket HFL samples.

II. METHODS

A. Stack deposition and magnetic characterization

The MTJ stacks were deposited on 300-mm wafers by Physical Vapour Deposition (PVD) in a Canon-Anelva EC7800. The reference layer (RL) and hard layer (HL) on top of the MgO consisted of CoFeB(11)/W(3)/Co(12)/Ru(8.5)/Co(6)/Pt(8)/[Co(3)/Pt(8)]₆/Ru(50) (thicknesses in Å). Blanket HFL samples were also sputtered on 300-mm wafers without the RL and HL. The non-magnetic capping layer on top of MgO consisted of CoFeB(5)/Mg(6.5)/Ta(30). All wafers were annealed after deposition at 300 °C for 30 min.

The anisotropy field was calculated as $\mu_0 H_k = 2K_{eff}/M_s$, where the saturation magnetization M_s and effective anisotropy energy density K_{eff} were measured by vibrating sample magnetometer (VSM). The DMI was measured by asymmetric bubble expansion with Kerr microscopy.^{18–20}

B. Fabrication and electrical characterization of MTJ devices

MTJ pillars were fabricated using standard MRAM processes.²¹ A buried bottom electrode contact (BEC) was used. Pillars were patterned by 193-nm immersion lithography and ion beam etching (IBE). Finally, Cu top contacts were fabricated.

MTJ properties were measured using an Hprobe platform, including TMR vs field and TMR vs STT voltage hysteresis loops using 50-ns voltage pulses.

C. He⁺ ion irradiation experiments

30-keV He⁺ irradiation was performed on 8 × 8 mm² blanket HFL samples with fluences ranging from 1 × 10¹⁴ to 2 × 10¹⁶ ions/cm².

III. RESULTS AND DISCUSSION

A. Hybrid free layer for full electrical control

We first study the properties of single HFL-MTJ pillars with 100-nm diameter. The stack consists of Pt/FL2/W/FL1/MgO, with reference and hard layers on top having fixed magnetization directions. A wedge along the wafer is used to vary either the thickness of FL1 = CoFeB in Figs. 2(a)–2(c), or the thickness of FL2 = Co in Figs. 2(d)–2(f).

Figures 2(b) and 2(c) show the MTJ properties as a function of the CoFeB thickness t_{CoFeB} [stack in Fig. 2(a)], where the TMR and the coercivity $\mu_0 H_c$ are obtained from field-driven hysteresis loops, while the switching voltage V_{sw} is obtained from STT-driven hysteresis loops. Those properties strongly depend on the CoFeB thickness. The TMR mainly improves as t_{CoFeB} increases, with values above 90% for $t_{CoFeB} > 7$ Å. Increasing further t_{CoFeB} leads to a decrease of the PMA indicated by the coercivity reduction and, as a result, a decrease of the switching voltage. $t_{CoFeB} \sim 8$ Å therefore provides a great balance between high readout signal and high PMA for reliable DW motion.

Fixing $t_{CoFeB} = 8$ Å, Figs. 2(e) and 2(f) show field-driven and STT-driven hysteresis loops for different Co thicknesses t_{Co} [stack in Fig. 2(d)]. We observe that the TMR is similar for the different thicknesses, while the coercivity and switching voltage increase for increasing t_{Co} . This corresponds to the increase of the PMA of the Co layer in this thickness range. For $t_{Co} > 10$ Å, the MTJ cannot be switched by STT due to the required voltage leading to the MgO barrier breakdown.

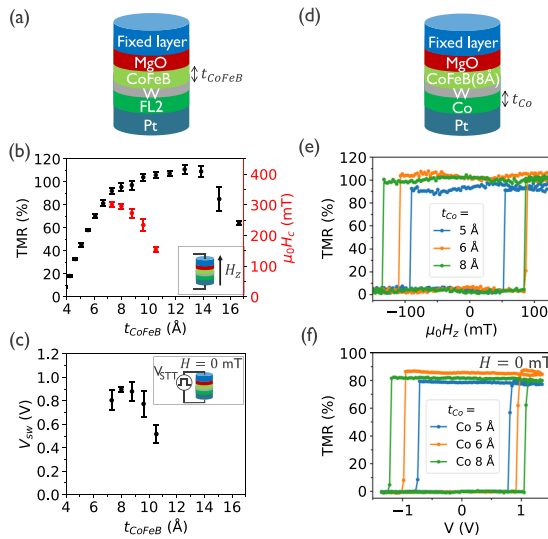


FIG. 2. (a) MTJ stack with a CoFeB wedge and FL2 = Co(8)/Ru(8.5)/Co(6) (thicknesses in Å). (b) TMR and free layer coercivity from field-driven loops as a function of CoFeB thickness for the stack of (a). (c) STT switching voltage (at zero field and for 50-ns voltage pulses) as a function of CoFeB thickness for the stack of (a). Error bars correspond to the standard deviation for multiple devices. (d) MTJ stack with $t_{\text{CoFeB}} = 8 \text{ \AA}$ and a wedge of FL2 = Co. TMR vs magnetic field loops (e), and TMR vs 50-ns voltage pulses loops (f), for different Co thicknesses for the stack of (d). Measurements on MTJ pillars with 100-nm diameter.

This study of MTJ properties highlights the potential to optimize FL2 while preserving MTJ read/write capabilities. This allows for the integration of high DMI materials, like Pt/Co, enabling fast DW motion and combining logic operations with electrical read/write functionalities.

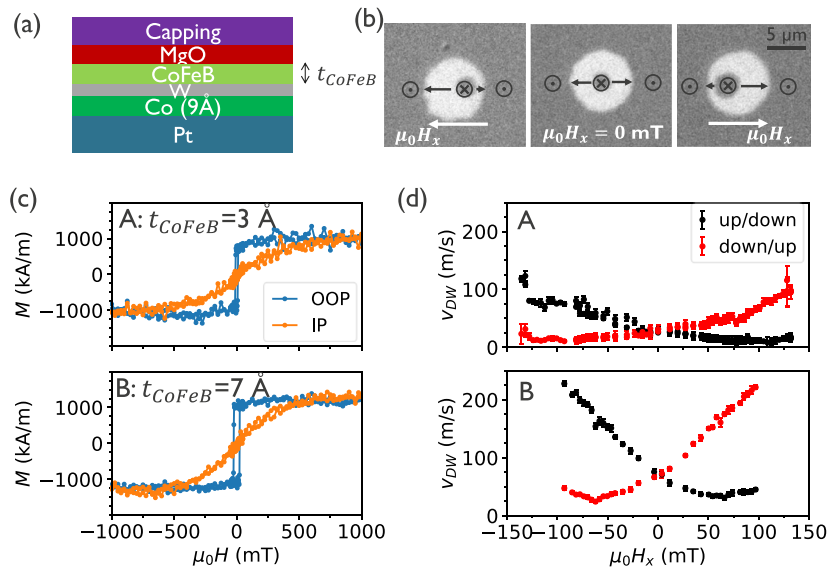


FIG. 3. (a) Blanket free layer stack for the DMI study. (b) Typical differential Kerr microscopy images of bubble expansion driven by OOP field pulses under a constant IP field (images for sample B). (c) OOP and IP VSM hysteresis loops of sample A and B. (d) Velocity of up/down and down/up DWs during field-driven expansion, as a function of the IP field (for sample A and B). Error bars correspond to the standard deviation of several measurements.

We now verify that the HFL stack based on Pt/Co provides adequate DMI such as in a single Pt/Co-based layer. We study two HFL blanket samples with stack Pt(50)/Co(9)/W(3)/CoFeB(t_{CoFeB})/MgO(10) with a capping layer [see Fig. 3(a)], where t_{CoFeB} is 3 Å for sample A and 7 Å for sample B. The Co thickness of 9 Å ensures high PMA in both samples to avoid uncontrolled magnetic domain nucleations due to the IP field applied during the measurement.

The differential Kerr images in Fig. 3(b) show a typical expansion of a bubble domain, driven by an OOP $\mu_0 H_z$ pulse with different IP fields $\mu_0 H_x$. To prevent the potential impact of DW pinning on the DMI measurement,^{18–20} we measure DW motion in the flow regime²² by applying $|\mu_0 H_z| > 150 \text{ mT}$ with pulse widths ranging from 20 to 40 ns. Clean domain nucleation and DW motion are observed. The asymmetric expansion of the bubble domain is due to the presence of chiral Néel DWs, whose velocity depends on the angle between the DW and the IP field. The DW velocity reaches a minimum when the IP field compensates the DMI field $\mu_0 H_{\text{DMI}}$ that stabilizes the chiral Néel DWs. The value of the DMI coefficient is then obtained by $|D| = \mu_0 H_{\text{DMI}} \Delta M_s$, with the domain wall parameter $\Delta = \sqrt{A/K_{\text{eff}}}$, where A and K_{eff} are the exchange constant and the effective anisotropy energy density, respectively. Here, we assume a constant value of $A = 16 \text{ pJ/m}$, typical for Pt/Co-based stacks.²³ Finally, the interfacial DMI coefficient is given by $D_s = Dt$ where t is the magnetic thickness (12 Å for sample A and 16 Å for sample B).

Figures 3(c) and 3(d) show the VSM hysteresis loops and DW velocity measurements for both samples, and the extracted parameters are given in Table I. From Fig. 3(c), we can see that the samples have PMA, and the extracted K_{eff} values in Table I are similar for both. From Fig. 3(d), we find DMI fields of 100 mT for sample A and 65 mT for sample B. The resulting DMI values are $|D| = 0.81 \pm 0.04 \text{ mJ/m}^2$ for $t_{\text{CoFeB}} = 3 \text{ \AA}$ and $|D| = 0.61 \pm 0.03 \text{ mJ/m}^2$

TABLE I. Measured magnetic properties for sample A and B: saturation magnetization M_s , effective anisotropy field $\mu_0 H_k$, effective anisotropy energy density K_{eff} , domain-wall parameter Δ , DMI field $\mu_0 H_{DMI}$, effective DMI coefficient D , effective interfacial DMI coefficient D_s .

Sample (thicknesses in Å)	M_s (kA/m)	$\mu_0 H_k$ (mT)	K_{eff} (kJ/m ³)	Δ (nm)	$\mu_0 H_{DMI}$ (mT)	$ D $ (mJ/m ²)	$ D_s $ (pJ/m)
A: Pt(50)/Co(9)/W(3)/CoFeB(3)/MgO(10)	1040 ± 10	500 ± 30	260 ± 20	7.8 ± 0.3	100 ± 3	0.81 ± 0.04	0.98 ± 0.04
B: Pt(50)/Co(9)/W(3)/CoFeB(7)/MgO(10)	1210 ± 7	440 ± 20	270 ± 10	7.7 ± 0.2	65 ± 3	0.61 ± 0.03	0.97 ± 0.05

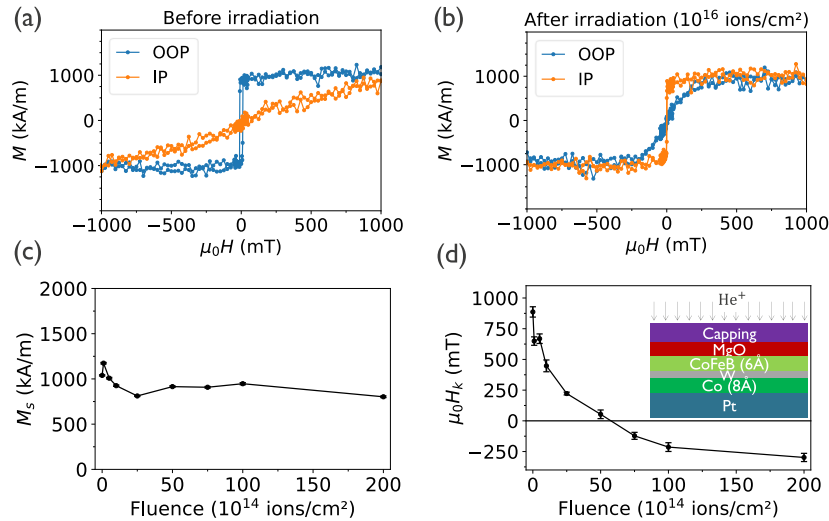


FIG. 4. OOP and IP VSM hysteresis loops before (a) and after (b) 30-keV He⁺ irradiation on the blanket stack of the inset in (d). Saturation magnetization (c) and anisotropy field (d) as a function of the fluence. Error bars are the standard error of the average due to noise.

for $t_{CoFeB} = 7$ Å. This leads to a similar interfacial DMI coefficient $|D_s| \sim 1$ pJ/m for both samples, indicating that the reduction of the D coefficient in sample B is mainly due to the increase of the magnetic thickness. This value of D_s is close to values in literature for Pt/Co/W and Pt/Co/Al stacks, ranging from 0.8 to 1.4 pJ/m.^{24,25}

This DMI study shows that the Pt/Co/W/CoFeB/MgO stack exhibits the effective DMI required to have chiral DWs for SOT-driven DW motion (see Fig. S1 in supplementary material) and for logic operation by chiral coupling,⁸ while MTJ write/read is enabled by the CoFeB/MgO layer.

B. He⁺ irradiation treatment for DW logic

We now investigate He⁺ ion irradiation as a treatment to convert the double free layer stack from PMA to IP, enabling DW logic. Indeed, to be compatible with PMA MTJ write/read, a treatment to convert from PMA to IP is required, as well as a stack which is switchable by STT. During the irradiation, He⁺ ions traverse the magnetic layers and are implanted deep into the substrate, inducing gentle atomic displacements at the interfaces, leading to a loss of the interfacial PMA.^{14,15}

We performed 30-keV He⁺ irradiation globally on blanket HFL samples of stack Pt(50)/Co(8)/W(3)/CoFeB(6)/MgO(10) with a capping layer (thicknesses in Å). Figures 4(a) and 4(b) show typical VSM measurements before and after the irradiation, indicating a conversion from PMA to IP anisotropy, even for an initial HFL stack

with high PMA. Figures 4(c) and 4(d) show the saturation magnetization M_s and anisotropy field $\mu_0 H_k$ as a function of the fluence. The saturation magnetization varies between 800 and 1200 kA/m and is only slightly affected even for very high fluences. We find that the anisotropy field is gradually converted from 890 ± 40 mT to -300 ± 30 mT at 2×10^{16} ions/cm².

This treatment therefore allows to precisely tune the anisotropy while keeping good saturation magnetization.

IV. CONCLUSION

In summary, we showed a viable approach toward the practical implementation of nanoscale DW logic devices. This is achieved through a flexible magnetic stack design to allow for the integration of MTJ write/read operations and efficient DW motion, as well as a reliable treatment to control the magnetic anisotropy of the stack from PMA to IP.

The stack consists of Pt/Co coupled with CoFeB/MgO through a W spacer. Our investigation revealed that a CoFeB thickness within 7 to 10 Å results in high TMR readout and efficient STT-driven DW writing. Importantly, we demonstrated that the introduction of the high DMI Pt/Co layer into the stack provides effective DMI required for SOT-driven DW motion. For Co thicknesses of 8 to 9 Å, our findings indicated clean DW propagation and efficient switching by STT. Finally, we proved that He⁺ ion irradiation is a reliable

technique to convert Pt/Co-based coupled free layers from a PMA state to IP orientation. Remarkably, this conversion occurs while maintaining high values of saturation magnetization, thereby enabling the realization of nanoscale DW logic applications.

Local patterning of IP regions, essential for the implementation of electrically controlled DW logic circuits, can be achieved either with mask-based strategies or extending focused ion beam methods^{16,17} to the double free layer stack.

SUPPLEMENTARY MATERIAL

Field-free SOT-driven DW motion for the stack of sample A of Fig. 3 is shown in the supplementary material (Fig. S1).

ACKNOWLEDGMENTS

This work was performed as part of the imec IAP core CMOS and Exploratory Logic Program of Intel Corporation. B.V. acknowledges FWO-Vlaanderen for a Strategic Basic Research PhD fellowship (1S72223N). B.V. thanks Bart Caerts for his support with the He⁺ ion irradiation. K.T. acknowledges KUL C1 grant C14/18/074 and the FWO-FNRS Weave program.

AUTHOR DECLARATIONS

Conflict of Interest

The authors have no conflicts to disclose.

Author Contributions

B. B. Vermeulen: Conceptualization (equal); Formal analysis (equal); Investigation (equal); Writing – original draft (lead); Writing – review & editing (lead). **E. Raymenants:** Formal analysis (equal); Investigation (equal). **V. T. Pham:** Formal analysis (equal); Investigation (equal). **S. Pizzini:** Writing – review & editing (equal). **B. Sorée:** Supervision (equal). **K. Wostyn:** Project administration (equal). **S. Couet:** Project administration (equal). **V. D. Nguyen:** Conceptualization (equal); Writing – original draft (equal); Writing – review & editing (equal). **K. Temst:** Supervision (equal); Writing – review & editing (equal).

DATA AVAILABILITY

The data that support the findings of this study are available from the corresponding author upon reasonable request.

REFERENCES

¹D. E. Nikonov *et al.*, “Proposal of a spin torque majority gate logic,” *IEEE Electron Device Lett.* **32**, 1128–1130 (2011).

²S. Das *et al.*, “Beyond CMOS,” in *2021 IEEE International Roadmap for Devices and Systems Outbriefs* (IEEE, 2021).

³E. Raymenants *et al.*, “Nanoscale domain wall devices with magnetic tunnel junction read and write,” *Nat. Electron.* **4**, 392–398 (2021).

⁴E. Raymenants *et al.*, “Magnetic domain walls: From physics to devices,” in *2021 IEEE International Electron Devices Meeting (IEDM)* (IEEE, 2021).

⁵I. M. Miron *et al.*, “Perpendicular switching of a single ferromagnetic layer induced by in-plane current injection,” *Nature* **476**, 189–193 (2011).

⁶S. Emori *et al.*, “Current-driven dynamics of chiral ferromagnetic domain walls,” *Nat. Mater.* **12**, 611–616 (2013).

⁷A. Thiaville *et al.*, “Dynamics of Dzyaloshinskii domain walls in ultrathin magnetic films,” *Europhys. Lett.* **100**, 57002 (2012).

⁸Z. Luo *et al.*, “Current-driven magnetic domain-wall logic,” *Nature* **579**, 214–218 (2020).

⁹I. Dzyaloshinsky, “A thermodynamic theory of ‘weak’ ferromagnetism of antiferromagnetics,” *J. Phys. Chem. Solids* **4**, 241–255 (1958).

¹⁰T. Moriya, “Anisotropic superexchange interaction and weak ferromagnetism,” *Phys. Rev.* **120**, 91–98 (1960).

¹¹Z. Luo *et al.*, “Chirally coupled nanomagnets,” *Science* **363**, 1435–1439 (2019).

¹²E. Liu *et al.*, “Top-pinned STT-MRAM devices with high thermal stability hybrid free layers for high-density memory applications,” *IEEE Trans. Magn.* **54**, 3401805 (2018).

¹³S. Ikeda *et al.*, “A perpendicular-anisotropy CoFeB/MgO magnetic tunnel junction,” *Nat. Mater.* **9**, 721–724 (2010).

¹⁴C. Chappert *et al.*, “Planar patterned magnetic media obtained by ion irradiation,” *Science* **280**, 1919–1922 (1998).

¹⁵T. Devolder *et al.*, “Magnetic properties of He⁺-irradiated Pt/Co/Pt ultrathin films,” *Phys. Rev. B* **64**, 064415 (2001).

¹⁶R. Juge *et al.*, “Helium ions put magnetic skyrmions on the track,” *Nano Lett.* **21**, 2989–2996 (2021).

¹⁷C. Balan *et al.*, “Improving Néel domain walls dynamics and skyrmion stability using He ion irradiation,” *Small* **19**, 2302039 (2023).

¹⁸S.-G. Je *et al.*, “Asymmetric magnetic domain-wall motion by the Dzyaloshinskii–Moriya interaction,” *Phys. Rev. B* **88**, 214401 (2013).

¹⁹A. Hrabec *et al.*, “Measuring and tailoring the Dzyaloshinskii–Moriya interaction in perpendicularly magnetized thin films,” *Phys. Rev. B* **90**, 020402 (2014).

²⁰M. Vaňatka *et al.*, “Velocity asymmetry of Dzyaloshinskii domain walls in the creep and flow regimes,” *J. Phys.: Condens. Matter* **27**, 326002 (2015).

²¹S. Rao *et al.*, “STT-MRAM array performance improvement through optimization of ion beam etch and MTJ for last-level cache application,” in *2021 IEEE International Memory Workshop (IMW)* (IEEE, 2021).

²²J. P. Garcia *et al.*, “Magnetic domain wall dynamics in the precessional regime: Influence of the Dzyaloshinskii–Moriya interaction,” *Phys. Rev. B* **104**, 014405 (2021).

²³T. Ha Pham *et al.*, “Very large domain wall velocities in Pt/Co/GdOx and Pt/Co/Gd trilayers with Dzyaloshinskii–Moriya interaction,” *Europhys. Lett.* **113**, 67001 (2016).

²⁴Y.-K. Park *et al.*, “Interfacial atomic layers for full emergence of interfacial Dzyaloshinskii–Moriya interaction,” *NPG Asia Mater.* **12**, 38 (2020).

²⁵F. Ajejas *et al.*, “Element-selective modulation of interfacial Dzyaloshinskii–Moriya interaction in Pt|Co|metal based multilayers,” *arXiv:2109.00761* (2021).